A Review of the Optical Properties of Biological Tissues

WAI-FUNG CHEONG, SCOTT A. PRAHL, AND ASHLEY J. WELCH, SENIOR MEMBER, IEEE

Abstract—**A comprehensive compilation of published optical properties (absorption, scattering, total attenuation, effective attenuation, and/or anisotropy coefficients) of various biological tissues at a variety of wavelengths is presented. The theoretical foundations for most experimental approaches are outlined. Relations between Kubelka–Munk parameters and transport coefficients are listed. The optical properties of aorta, liver, and muscle at 633 nm are discussed in detail.**

I. Introduction

THE propagation of laser light in tissue is a question of growing concern in many medical applications. Numerous models that predict fluence rates in tissue, or reflection and transmission of light by tissue have been developed. The accuracy of these models ultimately depends upon how well the optical properties of the tissue are known. Optical parameters are obtained by converting measurements of observable quantities (e.g., reflection) into parameters which characterize light propagation in tissue. The conversion process is based on a particular theory of light transport in tissue.

In past years, a host of investigators have reported values for the total attenuation coefficient, the effective attenuation coefficient, the effective penetration depth, the absorption and scattering coefficients, and the scattering anisotropy factor for a variety of tissues at a variety of light wavelengths. The majority of these results are based upon approximations to the radiative transport theory (e.g., diffusion theory). Yet sufficient variations in 1) model assumptions (e.g., isotropic–anisotropic scattering or matched–mismatched boundaries), 2) measurement techniques, 3) experimental apparatus, 4) calibration schemes, and 5) biological heterogeneities exist that efforts to extract average values for different tissue types is complicated. Regardless of these problems, there is a need to consolidate what has already been measured, and the main thrust of this paper is to present a summary of reported optical measurements. All published (within the authors' awareness) optical properties of tissue are gathered into this single compilation.

Manuscript received February 2, 1990; April 20, 1990. This work was supported in part by the Office of Naval Research under Contract N000014-86-K-0875 and by the Albert and Clemmie Caster Foundation, and was done at the University of Texas at Austin.

W.-F. Cheong was with the Biomedical Engineering Program, University of Texas at Austin, Austin, TX 78712. She is now with the Department of Dermatology, Boston University School of Medicine, Boston, MA 02118.

S. A. Prahl is with the Wellman Laboratories of Photomedicine, Harvard Medical School, Massachusetts General Hospital, Boston, MA 02114.

A. J. Welch is with the Department of Electrical and Computer Engineering, University of Texas at Austin, Austin, TX 78712.

IEEE Log Number 9040290.

A brief description of the radiative transport equation which is basic to all the light propagation models, and its associated parameters appears in Section II. Various solutions are presented to show how optical properties can be determined from using different measurements. Section III compares the Kubelka–Munk coefficients and the transport coefficients. Section IV provides specific descriptions of several methods used to determine optical properties. Section V discusses the measured optical properties for three selected tissue groups at 633 nm.

II. Light Propagation Models

Most of the recent advances in describing the transfer of laser energy in tissue are based upon transport theory. This theory is preferred in tissue optics instead of analytic approaches using Maxwell equations because of inhomogeneity of biological tissue. According to transport theory, the radiance $L(\boldsymbol{r}, \boldsymbol{s})$ ($\mathrm{W \cdot m^{-2} \cdot sr^{-1}}$) of light at position $\boldsymbol{r}$ traveling in a direction of the unit vector $\boldsymbol{s}$ is decreased by absorption and scattering but it is increased by light that is scattered from $\boldsymbol{s}'$ directions into the direction $\boldsymbol{s}$. The radiative transport equation which describes this light interaction is [1]

$$\boldsymbol{s} \cdot \nabla L(\boldsymbol{r}, \boldsymbol{s}) = -(\mu_a + \mu_s) L(\boldsymbol{r}, \boldsymbol{s}) + \mu_s \int_{4\pi} p(\boldsymbol{s}, \boldsymbol{s}') L(\boldsymbol{r}, \boldsymbol{s}')\, d\omega' \quad (1)$$

where $\mu_a(\mathrm{m^{-1}})$ is the absorption coefficient, $\mu_s(\mathrm{m^{-1}})$ is the scattering coefficient, $\mu_t(\mathrm{m^{-1}})$ is the attenuation coefficient, $d\omega'$ is the differential solid angle in the direction $\boldsymbol{s}'$, and $p(\boldsymbol{s}, \boldsymbol{s}')$ is the phase function. The total attenuation coefficient is

$$\mu_t = \mu_a + \mu_s. \quad (2)$$

The phase function describes the angular distribution for a single scattering event. For tractability, the phase function is usually assumed to be a function only of the angle between $\boldsymbol{s}$ and $\boldsymbol{s}'$. If the integral of the phase function is normalized to equal one, then $p(\boldsymbol{s}, \boldsymbol{s}')$ is the probability density function for scattering from direction $\boldsymbol{s}'$ to direction $\boldsymbol{s}$,

$$\int_{4\pi} p(\boldsymbol{s}, \boldsymbol{s}')\, d\omega' = 1 \quad (3)$$

Usually the form of the phase function is not known. In these cases the phase function is usually characterized by a single parameter g called the average cosine of the phase

function g,

$$g = \int_{4\pi} p(s, s')(s \cdot s')\, d\omega'. \tag{4}$$

This parameter is sometimes called the anisotropy coefficient. It is a measure of the asymmetry of the single scattering pattern; g approaching 1, 0, and -1 describes extremely forward, isotropic, and highly backward scattering, respectively.

Formulation of the transport equation assumes that each scattering particle is sufficiently distant from its neighbors to prevent interactions between successive scattering effects. In theory, these scatterers and absorbers must be uniformly distributed throughout the medium. Fluorescence and polarization events are neglected. Until recently, most tissue optics studies considered only steady-state (time-independent) transport of light.

Calculations of light distribution based on the radiative transport equation require knowledge of the absorption and scattering coefficients, and the phase function. Yet to arrive at these parameters, one must first have a solution of the radiative transport equation. Because of the difficulty of solving the transport equation exactly, several approximations have been made regarding the representation of the radiance and/or of the phase function. Forms of these approximate solutions for calculating light distribution within tissues are dependent upon the type of irradiance (diffuse or collimated) and the optical boundary conditions (matched or unmatched indexes of refraction). Fortunately, two simple solutions of the transport equation exist that provide expressions for the unscattered transmission and for the asymptotic fluence rate deep in a bulk tissue (far from light sources and boundaries).

A. Unscattered Transmission

Unscattered light is attenuated exponentially following Beer's law. For light passing through a slab of tissue with thickness t and having no reflections at the surface, the transmission is given by

$$T_c = e^{-\mu_t t} \tag{5}$$

where T_c is the unscattered transmission (sometimes also referred to as the collimated or the primary transmission). Thus the total attenuation coefficient can be obtained from a tissue sample using

$$\mu_t = -\frac{1}{t} \ln T_c. \tag{6}$$

If measurements of T_c are made when surface reflections are present, e.g., in air, corrections are required for the reflections at all mismatched surfaces. For a tissue sample placed between glass or quartz slides, the collimated beam is reflected at the air–slide, slide–tissue, tissue–slide, and slide–air interfaces. If the sample is only a few optical depths thick, multiple internal reflections must be considered. A net reflection coefficient for an air–glass–tissue layer is given by [2]

$$r = \frac{r_g + r_t - 2r_g r_t}{1 - r_g r_t} \tag{7}$$

where the Fresnel reflections at the air–glass and glass–tissue interfaces are r_g and r_t, respectively. The measured transmission $\boldsymbol{T}$ is

$$\boldsymbol{T} = \frac{(1 - r)^2}{1 - r^2 T_c^2} T_c. \tag{8}$$

Equation (8) is first solved for T_c, before using (6) to calculate μ_t.

B. Asymptotic Fluence Rate

In tissue regions far from light sources and boundaries, the fluence rate ($W \cdot m^{-2}$) decays exponentially. This is the dominant mode of propagation in an unbounded medium [3] and is often called the diffusion mode. The rate of decay is called the effective attenuation coefficient (μ_{eff}) or the diffusion exponent. An expression for this asymptotic fluence rate is

$$\Phi(z) \sim (\text{constant}) e^{-\mu_{\text{eff}} z} \tag{9}$$

In this paper, μ_{eff} will always refer to the *measured* rate of decay of the fluence in this diffusion region. An approximate relation for the effective attenuation coefficient in terms of the absorption, scattering, and anisotropy scattering coefficients is given below.

C. Diffusion Theory

The radiance in (1) can be separated into unscattered and scattered components

$$L(\boldsymbol{r}, s) = L_c(\boldsymbol{r}, s) + L_d(\boldsymbol{r}, s). \tag{10}$$

The unscattered portion (L_c) contains all light that has not interacted with the tissue. It satisfies Beer's law and the transmission equation (5). The scattered portion contains all light that has been scattered at least once and can be expressed exactly with an infinite sum of Legendre polynomials. However, the diffusion approximation truncates this sum to the first two terms (an isotropic and a slightly-forward directed term). This approximation simplifies the transport equation to the more tractable diffusion equation [4]

$$(\nabla^2 - \kappa^2)\Phi(\boldsymbol{r}) = -Q_0(\boldsymbol{r}) \tag{11}$$

where $\Phi(\boldsymbol{r})$ is the total scattered (diffuse) fluence rate given by

$$\Phi(\boldsymbol{r}) = \int_{4\pi} L_d(\boldsymbol{r}, s)\, d\omega. \tag{12}$$

The source term $Q_o(\boldsymbol{r})$ is generated by scattering of collimated normal irradiation

$$Q_o(\boldsymbol{r}) = -3\mu_s[\mu_a + \mu_s(1 - g) + \mu_t g] \cdot (1 - r_s)F_o(\boldsymbol{r}) \exp(-\mu_t z). \tag{13}$$

Here F_0 is the irradiance ($W \cdot m^{-2}$). The constant κ in (11) is an approximation of the actual measured effective attenuation coefficient μ_{eff} when absorption is dominated by scattering.

$$\kappa^2 = 3\mu[\mu_a + (1 - g)\mu_s]. \tag{14}$$

For diffuse irradiances, Q_o is typically set to zero because the diffuse incidence is introduced in the boundary conditions. The accuracy of the diffusion equation is affected by the ratio of scattering to absorption, the scattering anisotropy, and the distance from light sources and boundaries [5].

Several phase functions are compatible with the diffusion approximation: the isotropic [6], the delta–isotropic, the Eddington [7], and the delta–Eddington [8]. These functions are approximations of the actual phase function for tissue, e.g., the Henyey–Greenstein function for dermal and aortic tissues [2], [9]. In the diffusion approximation, the delta–Eddington phase function is the best function for simulating light transport in tissues characterized by Henyey–Greenstein scattering [10]. If g_{HG} is the average cosine of the Henyey–Greenstein phase function [3], then the diffusion equation for a delta–Eddington phase function is found by making the following substitutions in (11).

$$\frac{g_{HG}}{(1 + g_{HG})} \rightarrow g \tag{15a}$$

$$\mu_s(1 - g_{HG}^2) \rightarrow \mu_s. \tag{15b}$$

The solution of the diffusion equation (1) for the total fluence rate in a finite parallel slab is [4]

$$\Phi_{total}(z) = a_1 \exp(\kappa z) + a_2 \exp(-\kappa z) + a_3 \exp(-\mu_t z). \tag{16}$$

For a finite slab under plane collimated irradiation, Ishimaru provides values for a_1, a_2, and a_3 [4] for matched boundaries. In the case of a semi-infinite slab a_1 must equal zero; values for a_2 and a_3 have been evaluated by Phahl, based on the delta–Eddington approximation, for a uniform collimated irradiance F_0 for matched and mismatched boundary conditions [2].

The dominant term in (16) for large z in a semi-infinite slab yields the following approximate relation for the measured effective attenuation coefficient

$$\mu_{eff} \approx \kappa \quad \text{if } \mu_a \ll \mu_s. \tag{17}$$

The accuracy of this relation decreases with decreasing ratios of scattering to absorption and increasing anisotropy (see Table 23 in van de Hulst [4]) and fails completely when absorption dominates scattering (since both the limiting form of (16) changes and the diffusion approximation itself is inaccurate).

Expressions for light flux solutions of the diffusion equation (11) are

$$F_+(z) = \frac{a_1}{4}[1 - h\kappa]e^{\kappa z} + \frac{a_2}{4}[1 + h\kappa]e^{-\kappa z} + \left\{\frac{a_3}{4}[1 + h\mu_t] + \frac{\mu_s g(1 - r_s)F_0}{2[\mu_a + (1 - g)\mu_s]}\right\} e^{-\mu_t z} \tag{18a}$$

$$F_-(z) = \frac{a_1}{4}[1 + h\kappa]e^{\kappa z} + \frac{a_2}{4}[1 - h\kappa]e^{-\kappa z} + \left\{\frac{a_3}{4}[1 - h\mu_t] - \frac{\mu_s g(1 - r_s)F_0}{2[\mu_a + (1 - g)\mu_s]}\right\} e^{-\mu_t z} \tag{18b}$$

$$F_d(z) = F_+(z) - F_-(z). \tag{18c}$$

$F_+(z)$ and $F_-(z)$ are the forward and backward diffuse fluxes, respectively, and $F_d(z)$ is the net scattered flux along the direction of irradiation. The coefficient h is

$$h = 2/3[\mu_a + \mu_s(1 - g)]. \tag{19}$$

For a semi-infinite slab, both the fluence rate and the fluxes have the same exponential behavior for large z:

$$F_\pm(z) \sim \frac{a_2}{4}[1 \pm h\kappa]e^{-\kappa z} \quad \text{if } \mu_a \ll \mu_s. \tag{20}$$

Consequently, for highly scattering biological tissues, interstitial measurements of either fluence rate by isotropic detectors or flux by flat cut fibers placed deep inside the tissue permits evaluation of κ as suggested by (16) and (20) [11]–[14].

The reflection and transmission of a slab of thickness t with index matched boundaries in the diffusion approximation are given by [2], [4], [15], [16]

$$R = -\frac{\mu_s g}{[\mu_a + (1 - g)\mu_s]} + \frac{h}{2}\{a_1\kappa - a_2\kappa - a_3\kappa\} \tag{21a}$$

$$T = \frac{\mu_s g}{[\mu_a + (1 - g)\mu_s]} e^{-\mu_t t} - \{a_1\kappa e^{\kappa t} - a_2\kappa e^{-\kappa t} - a_3\mu_t e^{-\mu_t t}\}. \tag{21b}$$

The total transmission is $T_t = T + T_c$, where T_c is given by (5).

Measurements of diffuse reflection (R), total transmission (T_t), and unscattered transmission (T_c) provide sufficient information for uniquely determining three optical parameters (μ_a, μ_s, g). However, if only diffuse reflection and total transmission measurements are available, only absorption (μ_a) and reduced scattering [$\mu_s' = \mu_s(1 - g)$] coefficients can be calculated. The anisotropy (g) has been incorporated into μ_s' by the similarity relations $\mu_a' = \mu_a$ and $\mu_s'(1 - g') = \mu_s(1 - g)$. Anisotropic scattering is reduced to isotropic scattering by setting $g' = 0$ and so $\mu_s' = (1 - g)\mu_s$ [3], [17].

Some diffusion models incorporate index mismatched boundaries, scattering anisotropy, and tissue layers with varying optical properties. However, these models lead to complicated relations for reflection and transmission, and the optical properties cannot be directly expressed in terms of the reflection and transmission. Iterative methods (dis-

cussed in the next section) are used to determine optical properties using such models.

Several models proposed for modeling the propagation of laser light in tissue are listed in Table I along with the optical parameters required by each model. In particular, when a one-dimensional geometry is a reasonable representation, then the adding-doubling method [18]–[19] provides an accurate solution of transport equation for any phase function. This method permits modeling of anisotropically scattering, internally reflecting, and arbitrarily thick, layered media with relatively fast computations [3].

D. Kubelka-Munk Theory

The Kubelka–Munk theory describes the propagation of a uniform, diffuse irradiance through a one-dimensional isotropic slab with no reflection at the boundaries [20], [21]. This model is equivalent to a diffusion model having a forward and backward peaked phase function [3]. The Kubelka–Munk expressions for reflection and transmission of *diffuse* irradiance on a slab of thickness t are

$$R = \frac{\sinh(S_{KM} y t)}{x \cosh(S_{KM} y t) + y \sinh(S_{KM} y t)} \quad (22a)$$

$$T = \frac{y}{x \cosh(S_{KM} y t) + y \sinh(S_{KM} y t)} \quad (22b)$$

where A_{KM} and S_{KM} are the Kubelka–Munk absorption and scattering coefficients and have units of inverse length (m^{-1}). The parameters x and y are found using (23c). The advantage of the Kubelka–Munk model is that the scattering and absorption coefficients may be directly expressed in terms of the measured reflection and transmission

$$S_{KM} = \frac{1}{yt} \ln\left[\frac{1 - R(x - y)}{T}\right] \quad (23a)$$

$$A_{KM} = (x - 1) S_{KM} \quad (23b)$$

$$x = \frac{1 + R^2 - T^2}{2R}; \qquad y = +\sqrt{x^2 - 1}. \quad (23c)$$

The simplicity of the Kubelka–Munk model has made it a popular method for measuring the optical properties of tissue. Unfortunately, the assumptions of isotropic scattering, matched boundaries, and diffuse irradiance are atypical of the interaction of laser light with tissue. Despite attempts to extend the Kubelka–Munk model to collimated irradiance [16], [22], [23] and anisotropic scattering [15], [22], [25], this method remains a poor approximation for laser light propagation in tissue [24].

III. Transport and Kubleka–Munk Coefficients

Nearly all optical properties can be separated into either transport (μ_a, μ_s, g) or Kubelka–Munk (A_{KM}, S_{KM}) coefficients, based on the theory used to obtain them. Not surprisingly, transport properties correspond to theories based on the transport equation (e.g., the diffusion equation). Kubelka–Munk properties are obtained using (23) above.

TABLE I
Conversion Formulas Relating Kubelka–Munk to Transport Coefficients

Author	η	χ or χ' [1]	Restrictions [2]
Klier[3] [26]	$\frac{(1-\varphi)(1-a)}{(1+\varphi)\xi_0}$	$-\frac{a}{2\xi}\left(1-\frac{1}{\varphi}\right)$	*Isotropic* scattering,
van Gemert & Star[4] [27]	$\frac{(1-\varphi)(1-a')}{(1+\varphi)\xi_0}$	$-\frac{a'}{2\xi}\left(1-\frac{1}{\varphi}\right)$	*Anisotropic* scattering; delta-isotropic phase function
van Gemert & Star [27]	$\frac{1}{2}+\frac{1}{4}(1-a')$	$\frac{4}{3}+\frac{38}{45}(1-a')$	*Anisotropic* scattering, assumes $\mu_s \gg \mu_a$
Meador & Weaver [25]	$\frac{1}{2}+\frac{1}{4}(1-a)$	$\frac{4}{3}+\frac{38}{45}(1-a)$	*Isotropic* scattering; Delta-Eddington phase function (four moments)
Meador & Weaver [25]	$\frac{1}{2}$	$\frac{4}{3}+\frac{20}{45}(1-a)$	*Isotropic* scattering, Delta-Eddington phase function (two moments)
Brinkworth [28,29]	$\frac{1}{2}$	$\frac{4}{3}+\frac{80}{45}(1-a)$	*Isotropic* scattering, Eddington phase function

1 χ for isotropic and χ' for anisotropic scattering; $a=\mu_s/(\mu_s+\mu_a)$ and $a'=\mu_s(1-g)/[\mu_s(1-g)+\mu_a]$
2 All formulas assume index matched boundaries
3 $(\varphi^2-1)/2\varphi = (1+R^2-T^2)/2R$, and $\varphi = [\xi+\ln(1-\xi)]/[\xi-\ln(1-\xi)]$
4 $(\varphi^2-1)/2\varphi = (1+R^2-T^2)/2R$, and $\mu_s(1-g)/[\mu_s(1-g)+\mu_a] = [\xi+\ln(1-\xi)]/[\xi-\ln(1-\xi)]$

Transport coefficients can be derived from the collision of a plane wave with a particle [4]. Some of the wave is scattered, some is absorbed, and some is undisturbed. The absorption (σ_a) and scattering (σ_s) cross sections (m^2) for tissue are ill-defined, because the particles are not separated from one another. Consequently, with the notable exception of blood [4], these cross sections are not well defined and measured. However, the *volumetric* absorption and scattering coefficients (m^{-1}) can be defined by using (ρ) the average density of particles per unit volume of tissue (m^{-3}). The scattering coefficient is $\mu_s = \rho\sigma_s$ and the absorption coefficient is $\mu_a = \rho\sigma_a$. Note that the phase function is not involved in the description of the absorption and scattering coefficients.

The Kubelka–Munk parameters are defined by (22) and (23) above. In the given formulation, the fraction of light scattered forward is equal to the fraction scattered backward. Since the Kubelka–Munk formulas are based on a forward- and backward-peaked phase function, the equal scattering assumption is equivalent to assuming equal magnitudes for the phase function peaks. If these peaks had different magnitudes (as they should for anisotropic scattering), then two unequal scattering coefficients would result. The Kubelka–Munk scattering coefficients are thus dependent on the scattering anisotropy (or phase function) of the tissue.

A large number of investigators have used Kubelka–Munk theory to obtain optical properties. In response to this, several authors have attempted to relate the Kubelka–Munk coefficients to transport coefficients using the following relations [4], [25]–[29]:

$$\mu_a = \eta A_{KM} \tag{24a}$$

$$\mu_s = \chi S_{KM} \tag{24b}$$

$$\mu_s(1 - g) = \chi' S_{KM} \tag{24c}$$

Table I provides expressions for η and χ (or χ'). Only the relations of Klier [26] or van Gemert and Star [27] generate transport coefficients which lead to light distributions that agree with distributions based on exact solutions to the transport equation. Van Gemert and Star extend the isotropic relations of Klier to include anisotropic scattering. Both papers provide graphs of η and χ (or χ') as functions of $\mu_a/(\mu_s + \mu_a)$ and A_{KM}/S_{KM}. The usefulness of these relations is compromised because internal reflection in the slab is neglected. Such internal reflection effects can dramatically change the measured reflection and transmission [2]. A final set of transformations by Star is $A_{KM} = 2\mu_a$ and $S_{KM} = \{3\mu_s(1 - g) - \mu_a\}/4$ [30].

IV. Measurement of Optical Properties

A number of methods have been proposed for measuring the optical properties of tissues. These can be separated into two classes: *direct* and *indirect*. In *direct* techniques, optical properties are found using nothing more complicated than Beer's law. Unscattered transmission measurements [31], effective attenuation measurements [11]–[14], and goniophotometric measurements of the single scattering phase function [2], [9], [58] are direct techniques. In *indirect* techniques, a theoretical model of light scattering is used. Indirect techniques can be subdivided into iterative and noniterative methods. A *noniterative* method uses equations in which the optical properties are explicitly given in terms of the measured quantitites. The Kubelka–Munk and three-flux models are noniterative, indirect methods. In indirect *iterative methods*, the optical properties are implicitly related to measured quantities. The values for the optical properties are iterated until the calculated reflection and transmission match the measured values. These methods are the most cumbersome to use, but the optical model employed can be much more sophisticated than in the noniterative methods.

A. Direct Methods

Direct techniques do not depend on any specific model to obtain the optical parameter from measurements. Two optical parameters that are not dependent upon any specific model are the total attenuation coefficient μ_2 and the effective attenuation coefficient μ_{eff}. These parameters are determined using the following methods.

1) The total attenuation coefficient μ_t is obtained from measurements of unscattered transmission using (6), as depicted in Fig. 1(a). Thin slabs are employed [31]. Experimental data are most affected by beam geometry, sample characteristics, detection schemes, and multiple reflections at boundaries. This measurement is conceptually simple, but difficult to implement because of problems in separating on-axis scattered light from unscattered light.

2) The effective scattering coefficient (μ_{eff}) or effective penetration depth ($\partial_{eff} = 1/\mu_{eff}$), is estimated from fluence rate measured by interstitial detectors and using (16) and (19), as depicted in Fig. 1(b) [11]–[14], [32]–[36]. This is the simplest and most commonly determined parameter (see Tables III and IV). Fiberoptic detectors must be located inside the diffusion region of irradiated bulk samples, far from sources and boundaries. It is crucial that the measurement field be in the diffusion region. Otherwise the orientation of the fiber with respect to incoming beam [9], [34], and its numerical aperture (flat cut versus isotropic fibertips [37]–[39]) will introduce measurement errors.

B. Noniterative Indirect Methods

Such approaches require simple expressions relating the optical properties to measured transmission and reflection (e.g., Kubelka–Munk equations). It is not surprising that the two methods presented involve using (23).

1) The first method employs calculations of Kubelka–Munk absorption and scattering coefficients (A_{KM}, S_{KM}) from measurements of diffuse reflection and transmission for diffuse irradiance, and use of (23), as depicted in Fig. 1(c). This method is strongly limited because a perfectly diffuse irradiating source is not readily available.

2) The second method utilizes determination of absorption, scattering, and anisotropy coefficients from diffuse transmission and reflection measurements using relations derived by van Gemert *et al.* [16]. Kubelka–Munk coefficients are first computed, then transformed into transport coefficients, and finally combined with a measurement of unscattered transmission to yield the three optical coefficients. The same limitations of method 1) apply here. Relations which correct for mismatched boundaries are also available [40].

Other noniterative methods have also been used. An example is the combination of the absorbance of a sample placed in an integrating sphere and angular phase function measurements [41]–[43]. Marijnissen *et al.* [37] combined measurements of angular radiance patterns with measurements of μ_{eff} to deduce μ_a, μ_s, and g. Yoon [9] used asymptotic measurements of total diffuse transmission for different sample thicknesses with collimated transmission and goniophotometric studies to obtain optical properties.

More recent methods include pulsed photothermal radiometry (PPTR) [44], photoacoustic effects [45], and time-of-flight (TOF) studies [46]. However, PPTR and photoacoustic methods have been demonstrated only for measuring absorption coefficient. These three newer techniques are noninvasive and therefore show promise for *in vivo* determination of optical properties.

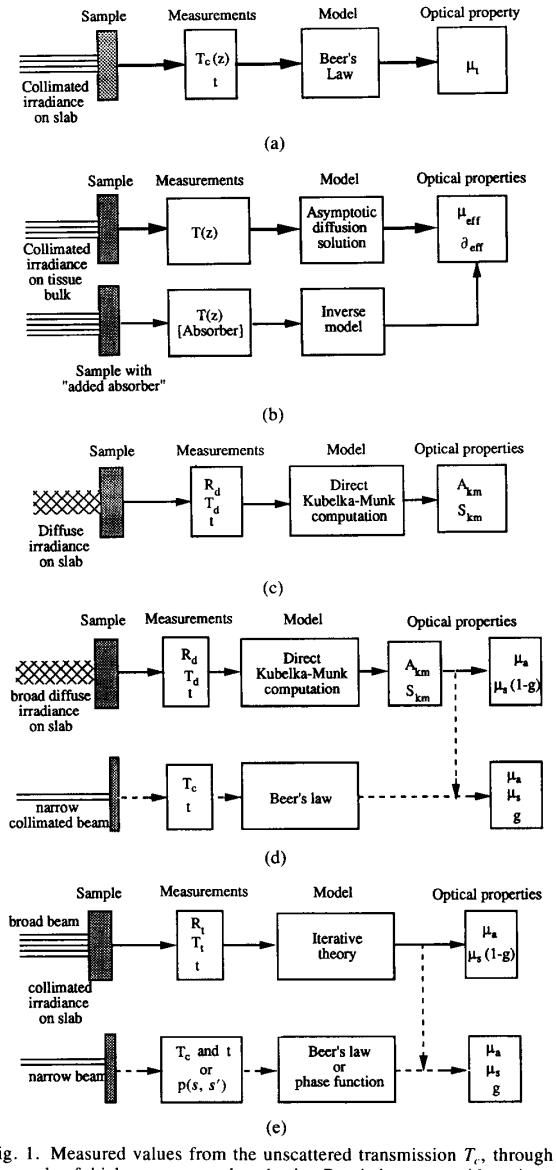

Fig. 1. Measured values from the unscattered transmission T_c, through a sample of thickness t are analyzed using Beer's law to provide estimates of the total attenuation coefficient (μ_t). (b) Interstitial measurements of fluence rate (or flux) inside a sample with or without an added absorber yield an estimate of the effective attenuation coefficient (μ_{eff}) or the effective penetration depth ($\partial_{eff} = 1/\mu_{eff}$). (c) Measurements of diffuse reflection R_d, and diffuse transmission T_d, and sample thickness t, for diffuse irradiance are used in (22) to compute Kubelka-Munk absorption A_{KM} and scattering S_{KM} coefficients. (d) Measurements of diffuse reflection and transmission for diffuse irradiance lead to Kubelka-Munk coefficients; these are then converted to transport parameters. When collimated transmission is available, μ_a, μ_s, and g can be calculated. (e) If only total reflection and transmission are available, the absorption coefficient μ_a and reduced scattering coefficient $\mu_s(1-g)$ can be determined with an iterative light transport model. An additional measurement (collimated transmission or the phase function) permits separate estimation of μ_a, μ_s, and g.

C. Iterative Indirect Methods

Unlike noniterative techniques, iterative procedures can use complicated solutions to the transport equations. Examples are diffusion theory, adding-doubling models [2], and Monte Carlo [47]. Typically, μ_a and $\mu_s(1-g)$ can be obtained if only total reflection and transmission are measured as shown in Fig. 1(e). If a third measurement of either the unscattered transmission or the phase function is available, then values for μ_a, μ_s, and g [or $p(s, s')$] can be determined. Iterative solutions usually include corrections for mismatched boundary conditions and/or for multiple layers. These methods often require two or more of the following measurements on a sample of known uniform thickness:

1) total (or diffuse) transmission for collimated or diffuse irradiance;
2) total (or diffuse) reflection for collimated or diffuse irradiance;
3) absorbance of the sample, placed inside an integrating sphere;
4) unscattered (collimated) transmission for collimated irradiation; and
5) angular distribution of emitted light from an irradiated sample.

Any three measurements from 1) to 5) would be sufficient to determine the three optical properties.

D. Sources of Errors

Computed values for the optical coefficients are inevitably prone to errors in all (or any) of the following:

1) physiological condition of the biological sample–hydration level, homogeneity, species variability, frozen–unfrozen state, *in vivo–in vitro*, fixed–unfixed, surface smoothness of the sample slabs;
2) irradiation geometry;
3) boundary index matching–mismatching;
4) orientation of detecting interstitial fibers with respect to source fiber;
5) numerical apertures of the sensing fibers;
6) angular resolution of the photodetectors;
7) separation of forward scattered light from unscattered light; and
8) theory used for the inverse problem.

These are important factors to consider when comparing optical properties obtained by different investigators.

V. Discussion

In recent years, many measurements of optical properties have been made. These optical properties can be used in the models listed in Table II. Tables III and IV are extensive lists of scattering, absorption, and anisotropy coefficients based on the transport theory. Table III lists the *in vitro* results, and Table IV tabulates optical properties measured *in vivo*. Each entry is accompanied by a brief description of the tissue preparation, sample geometry, experimental measurements and underlying theory. Kubelka–Munk coefficients are collected in Table V. Not all measurements listed in Tables III–V are discussed because of the wide variety of techniques and methods used. Instead, we concentrate on measurements of aorta, liver, and muscle at 633 nm and of liver tissue at 1060 nm.

A. Aorta

Aorta is a turbid tissue composed of interwoven elastin and collagen fibers, arranged in a trilayer structure of intima, media, and adventitia. Its appearance ranges from opaque white (porcine) to a pinkish-white in cadaveric samples.

Cadaveric aorta samples used by Yoon [9] were stripped to different thicknesses leaving mostly the intimal and media layers. Maintaining these samples in saline altered their hydration states. Keijzer *et al.* [48] froze samples to make microtome cuts. Despite these differences in sample preparation, Keijzer measured a scattering coefficient of 315 cm^{-1} and an anisotropy factor of 0.87 for normal media at 633 nm. These values agree closely with Yoon's values of $\mu_s = 310$ cm^{-1} and $g = 0.90$. In contrast, Keijzer's absorption coefficient of 2.3 cm^{-1} is higher than the $\mu_a = 0.52$ cm^{-1} value obtained by Yoon. If $\mu_a = A_{KM}/2$, then the A_{KM} values by van Gemert *et al.* [49] and Oraevsky *et al.* [50] for normal aorta are in closer agreement with the result by Yoon. Differences in treatment of internal reflections at the sample boundaries undoubtedly affected the computed absorption coefficients. Yoon fitted the asymptotic portion of a plot of diffuse transmission versus sample thickness to an equation that was independent of the tissue index of refraction, thus eliminating any need for boundary corrections. Keijzer, however, assumed a value for the refractive index to enable the inverse delta–Eddington program to correct for internal reflections. Another likely source for the descrepancy, was that by soaking the samples in saline, Yoon removed any remaining blood in the aorta sample, thereby reducing the measured absorption coefficient.

B. Liver

Unlike the aorta, liver tissues contain a dense population of erythrocytes within a vacuolar mesh of connective tissue and capillary beds. Absorption coefficients for liver range from 2.3–3.2 cm^{-1} at 633 nm. These are higher than those of other soft tissues. The reported absorption coefficients for liver agree within the errors introduced by interspecies variations. They also match the 1.3–2.7 cm^{-1} obtained for oxygenated whole blood by Pedersen *et al.* [51] and Reynolds *et al.* [52]. By comparison, the 6.5 cm^{-1} value for murine livers by Parsa using the delta–Eddington method is very high [53]. Here, index mismatching has been iteratively corrected in the inverse programs using assumed values for refractive indexes; Karagiannes *et al.* [54] adopted a similar approach. Marchesini *et al.* [43] and Andreola *et al.* [42] have not offered any clear details regarding their management of this problem. However, they did correct their absorbance measurements for multiple reflections associated with the integrating sphere, a correction ignored by other investigators. Without correction, the measured absorbance (or reflectance and transmission) exceeds the true absorbance.

TABLE II
FLUENCE MODELS WITH ASSOCIATED OPTICAL PARAMETERS

OPTICAL MODEL	OPTICAL COEFFICIENTS
I FLUX MODELS	
1. 2-Flux Kubelka-Munk (Kubelka [20-21])	A_{KM} and S_{KM}
2. 3-Flux (Atkins [22], van Gemert [16])	μ_a, μ_s, and g
3. 7-Flux (Yoon [9])	μ_a, μ_s, and g
II DIFFUSION MODELS	
1. Asymptotic (Svaasand [11], Profio [67]) Slab Symmetric sphere: Circular solid cylinder	μ_{eff} or $\partial_{eff} (= 0/\mu_{eff})$
2. Eddington (Ishimaru [4],)	μ_a, μ_s, and g
3. Delta-Eddington (Joseph [8], Prahl [2])	μ_a, μ_s, g' and f
III. P_n APPROXIMATION (Bell & Glasstone [68])	μ_a, μ_s, and p(s,s')
IV DISCRETE ORDINATE (Houf [69])	μ_a, μ_s, and p(s,s')
V. ADDING–DOUBLING (van de Hulst [18], Plass [19], Prahl [2])	μ_a, μ_s and p(s,s')
VI. MONTE CARLO (Wilson [70], Keijzer [71])	μ_a, μ_s, and p(s,s')

Scattering coefficients of 313 and 414 cm^{-1} were obtained, respectively, by Marchesini *et al.* [43] and Andreola *et al.* [42] for human liver at 633 nm. The scattering coefficient of 313 cm^{-1} is characteristic of values for soft tissues. However, Marchesini obtained a reduced scattering coefficient $\mu_s(1 - g)$ of 100.6 cm^{-1} that is significantly above the 5.23 cm^{-1} value reported by Kariagannes *et al.* [54] for bovine tissues and the 7.2 cm^{-1} value for murine samples measured by Parsa *et al.* [53]. This difference can be attributed to the measured anisotropy factor of 0.65 by Marchesini; it is substantially lower than reported values of 0.95 for rat liver by Parsa *et al.* [53] or values ranging 0.97 to 0.99 for blood by several authors [31], [55]–[57]. The coefficients determined by Marchesini also resulted in an approximate penetration depth of 33 μm. This suggests that two or more scattering events occurred within the 20–100 μm thick samples used in his goniometric studies to find the anisotropy factor. Jacques *et al.* [58] have demonstrated that the apparent anisotropy factor decreases as skin samples become thicker.

Measurements of effective attenuation coefficients (and effective penetration depths ∂_{eff}) are done in tissues far from sources and boundaries using isotropic detectors and/or flat cut fibers. These results should be functionally independent of detector geometry. Yet, measurements using the three orthogonal detectors described by Svaasand *et al.* [11] produced different attenuation coefficients for each detector. This suggests the measurements were made in regions with nonisotropic radiance distributions. The use of isotropic detectors [37]–[39], [59] may minimize these errors by recording an average and direction-independent signal. Also, measured μ_{eff} and calculated κ would not agree if (15a) is used outside its range of validity. Higher

TABLE III
OPTICAL PROPERTIES OF TISSUES *IN VITRO*

Tissue	λ	μ_t	μ_a	μ_s	$\mu_s(1-g)$	g	μ_{eff}	Tissue Preparation	Sample Geometry	Experimental Method	Theory	Reference
	nm	cm^{-1}	cm^{-1}	cm^{-1}	cm^{-1}		cm^{-1}					
Adipose												
Bovine	632.8	—	—	—	—	—	3.4	_____	thick slab	total T† using interstitial fiber detectors	diffusion theory	Preuss 1982 [13]
Porcine	630	376 (69)[a]	—	—	—	0.77	—	ground, frozen & sliced	very thin slab	direct T measurement, μ_t; goniophotometry	Beer's Law, Mie theory	Flock 1987 [31]
Aorta												
Human	632.8	316	0.52	316	41.0	0.87	—	freshly excised, kept in saline.	thin slab	diffuse T measurement, phase function with goniophotometry	asymptotic diffusion, Henyey-Greenstein (H-G) phase function	Yoon 1987 [9]
Human: Intima	476	252	14.8	237	45.0	0.81	—	excised, frozen & sliced	very thin slab	total T and R, unscattered T measurements	diffusion theory (Delta-Eddington)	Keijzer 1989 [48]
	580	191	8.9	183	34.8	0.81	—					
	600	182	4.0	178	33.8	0.81	—					
	633	175	3.6	171	25.7	0.85						
Human: Media	476	252	7.3	410	45.1	0.89	—	excised, frozen & sliced	very thin slab	total T and R, unscattered T measurements	diffusion theory (Delta-Eddington)	Keijzer 1989 [48]
	580	191	4.8	331	33.1	0.90	—					
	600	182	2.5	323	35.5	0.89	—					
	633	312	2.3	310	31.0	0.90						
Human: Adventitia	476	252	18.1	267	69.4	0.74	—	excised, frozen & sliced	very thin slab	total T and R, unscattered T measurements	diffusion theory (Delta-Eddington)	Keijzer 1989 [48]
	580	191	11.3	217	49.9	0.77	—					
	600	182	6.1	211	46.4	0.78	—					
	633	201	5.8	195	37.1	0.81						
Human	1060	—	2.0	—	—	—	—	_____	thick slab	magnitude of acoustic signal	photoacoustic	MacLeod 1988 [45]
Biliary Caculi (Gallstones)												
Porcinement	351	—	102 (16)	—	—	—	—	dehydrated, embedded in plastic, and sliced	~1 mm slab	thermal time response	pulsed photothermal radiometry	Long 1987 [44]
Stones	488	—	179 (28)	—	—	—	—					
	580	—	125 (29)	—	—	—	—					
	630	—	85 (11)	—	—	—	—					
	1060	—	121 (12)	—	—	—	—					
Cholesterol	351	—	88 (7)	—	—	—	—	dehydrated, embedded in plastic, and sliced	~1 mm slab	thermal time response	pulsed photothermal radiometry	Long 1987 [44]
Stones	488	—	62 (15)	—	—	—	—					
	580	—	36 (7)	—	—	—	—					
	630	—	44 (10)	—	—	—	—					
	1060	—	60 (9)	—	—	—	—					

† R = Reflectance, T = Transmission
[a] (± SD) standard deviation

TABLE III
OPTICAL PROPERTIES OF TISSUES *IN VITRO* (*CONTINUED*)

Tissue	λ	μ_t	μ_a	μ_s	$\mu_s(1-g)$	g	μ_{eff}	Tissue Preparation	Sample Geometry	Experimental Method	Theory	Reference
	nm	cm^{-1}	cm^{-1}	cm^{-1}	cm^{-1}		cm^{-1}					
Bladder												
Canine	630	59.6	0.6	59.0	8.85	0.85	—	———	spherical	μ_t, & radiance pattern with flat cut fibers; μ_{eff} with isotropic detectors	numerical transport solution by van de Hulst	Star 1987 [72]
Canine	633	52.0	1.25	50.8	2.54	0.95	—	excised and kept in saline	slab	diffuse R and T; axial transmission to get μ_t	3-flux model, transform KM to transport coeff.	Splinter 1989 [73]
Canine	632.8	45.1	1.10	44.0	3.52	0.92	—	~1 day post-resection, saline	slab	diffuse R and T; axial transmission to get μ_t	3-flux model, transform KM to transport coeff.	Cheong 1987 [74]
Human	632.8	89.4	1.40	88.0	3.52	0.96	—	~1 day post-resection, saline	slab	diffuse R and T; axial transmission to get μ_t	3-flux model, transform KM to transport coeff.	Cheong 1987 [74]
Human	633	30.7	1.40	29.3	2.64	0.91	—	excised and kept in saline	slab	diffuse R and T; axial transmission to get μ_t	3-flux model, transform KM to transport coeff.	Splinter 1989 [73]
Whole Blood												
Human HbO_2, Hct=0.41	685	1416	2.65	1413	—	0.99	—	diluted	——	radial distribution of reflection	transport theory	Pedersen 1976 [51]
Human HbO_2, Hct=0.41	665	1247	1.30	1246	6.11	0.995	—	non-hemolyzed, heparinized	cuvette	absorbance as function of sample thickness, angular light distribution	Mie theory	Reynolds 1976 [52]
	960	508	2.84	505	3.84	0.992	—					
Human Hb, Hct=0.41	665	514	4.87	509	2.49	0.995	—					
	960	670	1.68	668	5.08	0.992	—					
Human	633	29.0	—	—	—	0.974	—	diluted, non-hemolyzed	cuvette	unscattered T goniophotometry	Beer's Law Mie theory	Flock 1987 [31]
Canine	632.8	—	—	—	—	0.9845	—	heparinized	cuvette	goniophotometry	2-parameter phase function by Reynolds & McCormick [57]	Steinke [56]
	660	—	—	—	—	0.9840	—					
	800	—	—	—	—	0.980	—					

TABLE III
OPTICAL PROPERTIES OF TISSUES *IN VITRO* (*CONTINUED*)

Tissue	λ	μ_t	μ_a	μ_s	$\mu_s(1-g)$	g	μ_{eff}	Tissue Preparation	Sample Geometry	Experimental Method	Theory	Reference
	nm	cm^{-1}	cm^{-1}	cm^{-1}	cm^{-1}		cm^{-1}					
Brain												
Calf	633	—	0.19	—	6.6	—	3.4[b]	frozen	thin slab	total T and diffuse R	numerical iteration of	Karagiannes
	1064	—	0.36	—	6.7	—	2.5[b]	sections,	on glass		2-parameter phase fn.	1989 [54]
	1320	—	0.84	—	5.4	—	4.0	*post mortem*	slides		similarity transform	
Brain												
Bovine	630	—	—	—	—	—	2.5	*post mortem*	*in situ*	direct T with interstitial fiberoptic detectors	diffusion theory	Doiron 1983 [12]
Feline	488	—	—	—	—	—	10.9	*post mortem*	*in situ*	direct T with interstitial fiberoptic detectors	diffusion theory	Doiron 1983 [12]
	514.5	—	—	—	—	—	13.3					
	630	—	—	—	—	—	5.3-8.9					
Porcine	633	1037[c]	0.26	1037[c]	57.0	0.945[d]	6.7	———	thick slab *in situ*	direct T	diffusion theory "added absorber"	Wilson 1986 [14]
	633	—	—	—	—	—	4.3-14.2	*post mortem*	*in situ* thick slab (~40-50 mm)	direct T using two interstitial fiberoptic detectors	diffusion theory	Wilson 1985 [35]
	630	—	0.64	—	52.0	—	—	———	thick slab	direct T using interstitial fiber detectors	diffusion theory	Preuss 1982 [13]
	630	687	—	—	—	0.945	—	frozen & then thawed	thin slab	unscattered T; phase function with goniophotometry	Beer's Law for μ_t Mie theory	Flock 1987 [31]
Human: adult	488	—	—	—	—	—	14.0-25.0	1-2 days *post*	bulk tissue	total attenuation using	spherical diffusion	Svaasand & Ellingsen
	514	—	—	—	—	—	14.0-16.7	*mortem*, no fix,	(250 cm^3),	interstitial source and	theory	1983 [75]
	660	—	—	—	—	—	7.0-12.5	no irrigation of	*in situ*	fiberoptic detectors		
	1060	—	—	—	—	—	2.3-3.4	blood vessel				
	630	—	0.3-1.0	—	30.0-40.0	—	8.3	*post mortem*	slab	diffuse R and T; unscattered T	Kubelka-Munk to transport	Sterenborg 1988 [66]
Human: neonate	488	—	—	—	—	—	5.9-7.9	1-2 days post-	bulk tissue,	total attenuation using	spherical diffusion	Svaasand 1983 [75]
	514	—	—	—	—	—	5.8-9.0	mortem, no fix,	(250 cm^3),	interstitial source and	theory	
	660	—	—	—	—	—	2.5-3.3	no irrigation of	*in situ*	fiberoptic detectors.		
	1060	—	—	—	—	—	1.1-1.4	blood vessel				
Human:												
White matter	633	52.6	1.58	51.0	2.04	0.96	—	excised and	thin	diffuse R and T;	3-flux model	Splinter 1989 [73]
Grey matter	633	62.8	2.63	60.2	7.22	0.88	—	kept in saline	slab	unscattered T	KM to transport	

[b] Experimental measurement using interstitial fiberoptic detectors
[c] Calculated from g [ref. 31, Flock] and $\mu_s(1-g)$
[d] From reference [31], Flock 1987

TABLE III
OPTICAL PROPERTIES OF TISSUES *IN VITRO* (*CONTINUED*)

Tissue	λ	μ_t	μ_a	μ_s	$\mu_s(1-g)$	g	μ_{eff}	Tissue Preparation	Sample Geometry	Experimental Method	Theory	Reference
	nm	cm^{-1}	cm^{-1}	cm^{-1}	cm^{-1}		cm^{-1}					
Brain												
Canine												
White matter	633	92.2	2.02	90.2	6.31	0.93	—	excised and kept in saline	thin slab	diffuse R and T; unscattered T	3-flux model, transform KM to transport coeff.	Splinter 1989 [73]
Grey matter	633	58.0	1.65	56.3	1.97	0.97	—					
Brain Tumors												
Tumors	630	—	—	—	—	—	3.8-8.3	30-60 min. post-resection	*in situ*	direct T with interstitial fiberoptic detectors	spherical diffusion theory	Svaasand 1985 [77]
— glioma	630	—	5.0	—	7.0	—	—	*post mortem*	thin slab	diffuse R, diffuse T, unscattered T	transform KM into transport coefficients	Sterenborg 1988 [66]
— melanoma	630	—	—	—	8.0	—	—					
Breast Tissue												
Human: Fibrous	514	202	—	—	—	—	—	freshly resected	thin slab (~20μm) between glass	unscattered plus some (< 0.8 °) scattered T	Beer's law	Key 1988 [78]
	633	189	—	—	—	—	—					
	1060	165	—	—	—	—	—					
Human: Fatty	514	775	—	—	—	—	—	freshly resected	thin slab (~20μm) between glass	unscattered plus some (< 0.8 °) scattered T	Beer's law	Key 1988 [78]
	633	676	—	—	—	—	—					
	1060	524	—	—	—	—	—					
Human	635	—	≤ 0.2	395(35)[a]	—	—	—	frozen sections	very thin slab between glass	absorbance in integrating sphere, unscattered T from goniophotometry	Beer's law	Marchesini 1989 [43]
Heart												
Endocardium	1060	—	0.07	136	—	0.973	—	excised and kept in saline	thin slab	simultaneous diffuse R and T; unscattered T	3-flux model, transform KM to transport coeff.	Splinter 1989 [80]
Epicardium	1060	—	0.35	167	—	0.983	—	excised and kept in saline	thin slab	simultaneous diffuse R and T; unscattered T	3-flux model, transform KM to transport coeff.	Splinter 1989 [80]
Kidney												
Human	630	—	—	—	—	—	4.0	*post mortem*	thin slab	unscattered T	Beer's law	Eichler 1977 [33]
Bovine	630	—	—	—	—	—	7.9	————	*in situ*, thick slab	direct T using interstitial fiber detectors	diffusion theory	Preuss 1982 [13]
Kidney												
Porcine (cortex)	630	—	—	—	—	—	4.8	*post mortem*	*in situ*	direct T using interstitial fiberoptic detectors	diffusion theory	Doiron 1983 [12]

[a] (± SD) standard deviation

TABLE III
OPTICAL PROPERTIES OF TISSUES *IN VITRO* (*CONTINUED*)

Tissue	λ	μ_t	μ_a	μ_s	$\mu_s(1-g)$	g	μ_{eff}	Tissue Preparation	Sample Geometry	Experimental Method	Theory	Reference
	nm	cm^{-1}	cm^{-1}	cm^{-1}	cm^{-1}		cm^{-1}					
Liver												
Bovine	630	—	—	—	—	—	8.1	———	*in situ*, thick slab	direct T measurement with interstitial fiber detectors	diffusion theory	Preuss 1982 [13]
	633	—	3.21	—	5.23	—	6.8[b]	frozen sections, *post mortem*	thin slab between glass	total T and diffuse R	diffusion theory 2-parameter phase function	Karagiannes, 1989 [54]
	1064	—	0.53	—	1.76	—	3.2[b]					
	1320	—	0.70	—	1.2	—	2.0					
Human	630	—	—	—	—	—	11.0	*post mortem*	thin slab	unscattered T	Beer's law	Eichler 1977 [33]
	630	—	3.2	414	—	0.95[e]	—	*post mortem*	thin slab (0.05-0.2 mm)	absorbance in integrating sphere; goniophotometry	Beer's law	Andreola 1988 [42]
	635	315	2.3	313	—	0.68	26.6	frozen sections	thin slab between glass	absorbance in integrating sphere, unscattered T from goniophotometry	Beer's law	Marchesini, 1989 [43]
	515	304	18.9	285	—	—	—					
Murine (albino)	488	—	12.2	173.5	—	0.93	29.9	fresh and frozen sections	thin slab between glass slides	total T and total R unscattered T	diffusion theory (Delta-Eddington)	Parsa 1989 [53]
	633	—	6.5	143.7	—	0.95	16.3					
	800	—	5.7	97.0	—	0.94	14.0					
	1064	—	5.9	60.9	—	0.92	13.8					
	1320	—	6.6	44.2	—	0.91	14.5					
	2100	—	27.2	24.5	—	0.80	51.2					
Porcine	630	—	—	—	—	—	13.0	*post mortem*	*in situ*	direct T using interstitial fiberoptic detectors	diffusion theory	Doiron 1983 [12]
	630	—	2.7	—	17.0	—	—	———	*in situ*	direct T	diffusion theory	Wilson 1986 [34]
Rabbit	630	—	—	—	—	—	12.5	*post mortem*, surface moist	*in situ* ~15 mm thick	direct T using interstitial fiberoptic detectors	diffusion theory	Wilson 1985 [35]
	1060	—	10.0	—	—	—	—	———	thick slab	magnitude of acoustic signal	photoacoustic	MacLeod 1988 [45]
Lung												
Human lung substance, deflated	633	—	—	—	—	—	11.0	*post mortem*	*in situ*	direct T using interstitial fiberoptic detectors	diffusion theory	Doinon 1982 [62]
Squamous cell Carcinoma	633	—	—	—	—	—	6.3	*post mortem*	*in situ*	— as above —	— as above —	Doiron 1983 [12]
Bronchial mucosa	633	—	—	—	—	—	9.1	*post mortem*	*in situ*	— as above —	— as above —	Doinon 1982 [62]
Human: normal	630	—	8.4	35.9	—	0.95[c]	—	frozen, rehydrated	thin slab (0.05-0.2 mm)	absorbance in integrating sphere; goniophotometry	Beer's law	Andreola 1988 [42]

[b] Experimental measurement using interstitial fiberoptic detectors
[e] Averaged value

TABLE III
OPTICAL PROPERTIES OF TISSUES *IN VITRO* (*CONTINUED*)

Tissue	λ	μ_t	μ_a	μ_s	$\mu_s(1-g)$	g	μ_{eff}	Tissue Preparation	Sample Geometry	Experimental Method	Theory	Reference
	nm	cm^{-1}	cm^{-1}	cm^{-1}	cm^{-1}		cm^{-1}					
Lung												
Human: normal	635 515	332 380	8.1 25.5	324 356	— —	0.75 —	— —	frozen sections	thin slab between glass slides	absorbance in integrating sphere, unscattered T from goniophotometry	Beer's law	Marchesini 1989 [43]
Muscle												
Bovine	633	8.30	0.40	7.9	5.53	0.30	2.7	chopped	thick slab	μ_t, & radiance pattern with flat cut fibers; μ_{eff} with isotropic detectors	transport theory	Marijnissen 1987 [38]
	633	121[c]	1.50	119[c]	7.0	0.941[d]	6.2	———	thick slab	direct T	diffusion theory "added absorber"	Wilson 1986 [14]
Bovine	630	—	—	—	—	—	5.6	*post mortem*	*in situ*	direct T using interstitial fiberoptic detectors	diffusion theory	Doiron 1983 [12]
	630	—	—	—	—	—	6.9	*post mortem*	*in situ*	direct T measurement with interstitial fiber detectors	diffusion theory	Preuss 1982 [13]
	630	328 (37)[a]	—	—	—	0.941	—	ground, frozen & thawed	thin slab	direct T measurement; phase function with goniophotometry	Beer's law for μ_t Mie theory	Flock 1987 [31]
Bovine	630	—	3.5	45.0	—	—	5.9	———	bulk	isodoses recorded on photographic film, contours yield μ_{eff}	diffusion theory	McKenzie 1988 [39]
	630	—	—	—	—	—	4.3-5.6	———	———	———	diffusion theory	Bolin 1987 [63]
Bovine	633 1064 1320	— — —	1.7 1.2 2.3	— — —	4.4 2.8 2.4	— — —	3.9[b] 2.3[b] 5.6	frozen sections, *post mortem*	thin slab between glass slides	total T and diffuse R	Numerical iterations, 2-parameter phase func., similarity transform	Karagiannes 1989 [54]
Chicken	633	4.30	0.17	4.1	3.3	0.20	1.34	chopped	*in situ*	μ_t, & radiance pattern with flat cut fibers; μ_{eff} with isotropic detectors.	transport theory	Marijnissen & Star 1985 [59]
Chicken	633	230[c]	0.12	229[c]	8.0	0.965[d]	1.7	resected & coarsely ground	thick slab	direct T	diffusion theory "added absorber"	Wilson 1986 [14]

[c] calculated from g [ref.31] and $\mu_s(1-g)$
[d] From reference [31], Flock 1987
[a] (± SD) standard deviation
[b] Experimental measurement using interstitial fiberoptic detectors

TABLE III
OPTICAL PROPERTIES OF TISSUES *IN VITRO* (*CONTINUED*)

Tissue	λ	μ_t	μ_a	μ_s	$\mu_s(1-g)$	g	μ_{eff}	Tissue Preparation	Sample Geometry	Experimental Method	Theory	Reference
	nm	cm^{-1}	cm^{-1}	cm^{-1}	cm^{-1}		cm^{-1}					
Muscle												
Chicken	630	345 (42)[a]	—	—	—	0.965	—	ground, frozen & then thawed	thin slab	direct T measurement; phase function with goniophotometry	Beer's law Mie theory	Flock 1987 [31]
Human	515	541	11.2	530	—	—	—	frozen sections	thin slab between glass slides	absorbance with integrating sphere, unscattered T from goniophotometry	total attenuation	Marchesini 1989 [43]
Porcine	633	41.0	1.0	40.0	1.2	0.97	—	fresh & frozen sections	thin slab	total T and diffuse R	Monte Carlo	Wilksch 1984 [47]
	1060	—	2.0	—	—	—	—	———	thick slab	magnitude of acoustic signal	photoacoustic	MacLeod 1988 [45]
Rabbit	630	—	—	—	—	—	1.1-1.5	*post mortem*	*in situ*	direct T using interstitial fiberoptic detectors	spherical diffusion theory	Doiron 1983 [12]
	514.5	—	—	—	—	—	2.0-2.5	*post mortem*	*in situ*, bulk	— as above —	— as above —	Doinon 1982 [62]
Rabbit	630 514	— —	— —	— —	— —	— —	2.7-12.5 3.7-10.0	moist surface	*in situ*, thick ~30-40 mm	direct T measured interstitially	diffusion theory	Wilson 1985 [35]
Skin												
Human dermis	630	243	1.8	—	—	—	—	excised flaps	thin slab 0.05-0.2 mm	absorbance in integrating sphere; goniophotometry	Beer's law	Andreola 1988 [42]
Human dermis (Caucasian)	633	190	2.7	187	35.5	0.81	—	bloodless, 85% hydration, fresh & frozen	thin slab between glass	goniophotometry, total R and total T	diffusion theory Henyey-Greenstein phase function	Jacques 1987 [58]
Human dermis	635	—	1.8	244	—	—	—	frozen sections	thin slab between glass slides	absorbance in integrating sphere, unscattered T from goniophotometry	Beer's law	Marchesini 1989 [43]
Murine dermis (albino)	488	242	2.8	239	62	0.74	—	Fresh whole dermis	thin slab between glass slides	total R and total T: unscattered T	diffusion theory	Jacques 1987 [15]
Human stratum corneum	193	—	6000	—	—	—	—	frozen sections	thin slab	unscattered T as function of thickness	Beer's law	Watanabe 1988 [79]

[a] (± SD) standard deviation

TABLE III
OPTICAL PROPERTIES OF TISSUES *IN VITRO* (*CONTINUED*)

Tissue	λ	μ_t	μ_a	μ_s	$\mu_s(1-g)$	g	μ_{eff}	Tissue Preparation	Sample Geometry	Experimental Method	Theory	Reference
	nm	cm^{-1}	cm^{-1}	cm^{-1}	cm^{-1}		cm^{-1}					
Tumors												
Rat prostrate tumor (R3327–AT)												
	633	271	0.49	270.	8.1-5.4	.97-.98	3.6-2.9	excised, frozen & sectioned	thin slab (120 μm)	absorbance in integrating sphere; goniophotometry	diffusion theory	Arnfield 1988 [41]
Rat rhabdomyosarcoma												
	630	—	1.1	—	7.0	—	—	freshly excised	thin slab	diffuse R and T	KM converted to transport coefficients using equations [ref. 16]	van Gemert 1985 [81]
	514	—	2.3	—	11.1	—	—					
	405	—	42.9	—	24.8	—	—					
Human intracranial tumors (meningiomas, astrocytomas, glioblastomas)												
	488	—	—	—	—	—	7.1-20.0	freshly resected	tissue vol. ≈5-10 cm^3, *in situ*	*in situ* T with embedded fiberoptic detectors.	diffusion theory	Svaasand 1985 [77]
	514	—	—	—	—	—	7.1-20.0					
	635	—	—	—	—	—	5.9-3.9					
	1060	—	—	—	—	—	3.3-1.9					
Rabbit VX2	630	628(106)[a]	—	—	—	0.639	—	ground, frozen & then thawed	thin slab	direct T measurement; phase function with goniophotometry	Beer's Law Mie theory	Flock 1987 [31]
Murine sarcoma	630	—	—	—	—	—	2.3	*post mortem*	*in situ*	direct T using interstitial fiberoptic detectors orientated in 3 directions	diffusion theory	Doiron 1982 [62]
	514.5	—	—	—	—	—	4.8					
Murine fibrosarcoma												
	630	—	—	—	—	—	4.4-9.8	———	———	direct T with interstitial fiberoptics	Beer's law	Driver 1988 [36]
Uterus												
Human	635	394	0.35	394	—	0.69	—	frozen sections	thin slab between glass slides	absorbance in integrating sphere, unscattered T from goniophotometry	Beer's law	Marchesini 1989 [43]

[a] (± SD) standard deviation

TABLE IV
OPTICAL PROPERTIES OF TISSUES *IN VIVO*

Tissue	λ	μ_t	μ_a	μ_s	$\mu_s(1-g)$	g	μ_{eff}	Tissue Preparation	Sample Geometry	Experimental Method	Theory	Reference
	nm	cm^{-1}	cm^{-1}	cm^{-1}	cm^{-1}		cm^{-1}					
Brain												
Human	630	—	—	—	—	—	2.2-3.7	*in situ*	intact, spherical field	direct T measured during PDT, interstitially; irradiated with embedded inflated balloon light source	diffusion theory spherical solution	Wilson 1986 [82]
	630	—	—	—	—	—	4.8-10.0	*in situ*	intact	— as above —	— as above —	Muller 1986 [83]
Porcine	630	—	—	—	—	—	3.7-4.5	*in situ*	intact spherical field	direct T with distance from irradiation surface, interstitial fiberoptic detectors	diffusion theory	Wilson 1985 [35]
Brain tumors	630	—	—	—	—	—	2.4	*in situ*	intact	direct T at different distances from interstitial spherical source, post-PDT	diffusion theory spherical solution	Wilson 1986 [82]
	630	—	—	—	—	—	2.2-6.6	*in situ*	intact	— as above —	— as above —	Muller 1986 [83]
Cat	631	—	—	—	—	—	5.0-9.8	*in situ*	intact organ	direct T using interstitial fiberoptic detectors	diffusion theory	Doiron 1982
	577	—	—	—	—	—	25.9					
	545	—	—	—	—	—	34.4					
	405-410	—	—	—	—	—	44.1					
Liver												
Rabbit	630	—	—	—	—	—	9.0-25.0	*in situ*	intact	direct T with distance from irradiation surface, interstitial	diffusion theory	Wilson 1985 [35]
Muscle												
Rabbit	630	—	—	—	—	—	2.6-4.8	*in situ*	intact bulk ~30-40 mm	direct T using interstitial fiberoptic detectors	diffusion theory	Wilson 1985 [35]
	514	—	—	—	—	—	4.5-6.3					
	630	—	—	—	—	—	1.6-2.3	*in situ*	intact	direct T using interstitial fiberoptic detectors	diffusion theory	Doiron 1983, 1982
	514.5	—	—	—	—	—	4.8-7.7					
Tumors												
Human retinoblastoma in athymic mice	488/514	—	—	—	—	—	6.25	*in situ*	intact tissue	direct T measured with ball-tipped fiberoptics connected distally to photodiode	diffusion theory	Svaasand 1989 [76]
	630	—	—	—	—	—	3.03					
	668	—	—	—	—	—	2.8					
	1064	—	—	—	—	—	1.3					
Mammary carcinoma in C3H/HEJ mice	488/514	—	—	—	—	—	9.1	*in situ*	intact tissue	direct T measured with ball-tipped fiberoptics connected distally to photodiode	diffusion theory	Svaasand 1989 [76]
	630	—	—	—	—	—	5.0					
	668	—	—	—	—	—	4.3					
	1064	—	—	—	—	—	2.7					
B16 melanotic melanoma in C57/B16 mice	630	—	—	—	—	—	20.0	*in situ*	intact tissue	direct T measured with ball-tipped fiberoptics connected distally to photodiode	diffusion theory	Svaasand 1989 [76]
	668	—	—	—	—	—	20.0					
	1064	—	—	—	—	—	5.0					

TABLE V
KUBELKA-MUNK COEFFICIENTS *IN VITRO*

Tissue	λ nm	Σ [f] cm^{-1}	A_{km} cm^{-1}	S_{km} cm^{-1}	Tissue Preparation	Sample Geometry	Reference
Aorta (human)							
Normal	514.5	22.1	11.1(2.7)[a]	11.0(0.8)	Cadaver specimens;	slabs	van Gemert, 1985 [49]
	633	8.1	1.8(.9)	6.3(1.4)			
	1060	3.7	0.9(.3)	2.8(2.0)			
Normal	633	8.2[h]	2.0	16.0	Cadaver specimens	slabs	Oraevsky, 1988 [50]
	488	20.0[h]	7.8	21.7	2-6 hours *post mortem*		
Blood							
Human	514	140	125	15.0		cuvettes	van Gemert, 1985 [49]
	633	4.0	1.0	3.0		cuvettes	
	1060	7.0	4.0	3.0		cuvettes	
Plaque							
Human	514.5	37.0	18.0	19.0	Cadaver specimens	slabs	van Gemert, 1985 [49]
	633	14.0	2.0	12.0	(heterogenous plaque)		
	1060	3.7	1.4	2.3			
Fibrous	633	10.1[h]	2.5	19.2	Cadaver specimens	slabs	Oraevsky, 1988 [50]
	488	30.1[h]	16.6	19.0	2-6 hours *post mortem*		
Skin (human)							
Dermis	630	65.0	5.0	60.0	Frozen sections	slabs	Anderson, 1981 [84]
Dermis [g]	415	_	20.0	138		slabs	van Genert, 1986 [85]
	500	_	11.3	90.8			
	540	_	9.0	78.0			
	577	_	7.5	69.0			
	694	_	6.8	55.3			
	1060	_	6.0	35.0			
Dermis (breast & abdominal skin)	630	60.0	20	40	In 60°C water to separate dermis from epidermis	slabs	Wan, 1981 [86]
Epidermis [g]	415	_	51.7	44.0		slabs	van Genert, 1986 [85]
	500	_	36.7	36.7			
	540	_	33.3	33.3			
	577	_	30.0	30.0			
	694	_	26.7	24.0			
	1060	_	20.0	16.0			

[f] Total attenuation coefficient $\Sigma = A_{km} + S_{km}$
[a] (± SD) standard deviation
[h] Effective attenuation coefficient = $\sqrt{(A_{km}^2 + 2A_{km} S_{km})}$
[g] Absorption and scattering coefficients derived from original spectra produced by Wan et. al [86] and Anderson et. al [84], and compiled in figure 1 of reference [85]; tabulated values are digitized from plots in this figure 1.

μ_{eff} values were obtained directly from interstitial fluence measurements [12], [13], [33]–[35] than those calculated from μ_a and $\mu_s(1 - g)$ parameters for bovine (Karagiannes), human (Marchesini), and murine (Parsa) livers.

At 1060 nm, absorption coefficients of 10 cm^{-1} for rabbit liver by MacLeod *et al.* [45] using photoacoustic spectroscopy and 0.53 cm^{-1} for bovine liver by Karagiannes using diffuse reflection and transmission are reported. The 10 cm^{-1} value seems high, even allowing for biological variations among species, since it is about twice the 5.5 cm^{-1} value obtained for arterial clots by Cheong [60]. A possible cause is the 1 cm spatial resolution in the photoacoustic studies. Another possibility is the inclusion of scattering effects in the absorbance measurements. Scattering redistributes the light over a broader tissue volume, effectively increasing the pathlength for optical absorption, and hence a larger absorption coefficient would be measured. In fact, examination of Table III reveals that absorption parameters measured by photoacoustic means are generally higher than those made with other techniques.

C. Muscle

Bovine muscles absorb more light at 633 nm (μ_a = 1.5–3.5 cm^{-1}) than the whiter chicken muscles (0.17–0.12 cm^{-1}) but less than the better perfused human mus-

cles (11.2 cm^{-1}). Marijnissen *et al.* [37] report an absorption coefficient of 0.4 cm^{-1} for bulk bovine muscle; this is significantly less than the 1.5 cm^{-1} from Wilson *et al.* [14] using the "added absorber" technique, or the 3.5 cm^{-1} value from McKenzie [39] based on fitting isodose contours on exposed photographic films to diffusion theory. These variations are typical of optical properties reported by different authors. Both Marijnissen and McKenzie used isotropic sensors in their measurements. Wilson used finite aperture detectors. Nevertheless, a large difference exists between the results by Marijnissen and the values by McKenzie. The absorption coefficients by Wilson and Marijnissen are more consistent and are typical of soft tissues at 633 nm. Marchesini's [43] direct measurement of absorbance of a sample placed inside an integrating sphere yielded a high value of 11.2 cm^{-1} for human tissues. Absorbance determined in this way is generally overestimated because scattering increases the average photon pathlength.

Marchesini *et al.* reported a scattering coefficient of 530 cm^{-1}, which is higher than other values in Table III. The 4.1 and 7.9 cm^{-1} values reported for bovine and chicken muscle by Marijnissen *et al.* [59] are extremely low. Star *et al.* attributes this to large detecting apertures [61]. In early studies it was not realized that tissues were highly forward scattering, as shown later by the 0.97 and 0.94 reported for g by Wilksch *et al.* [47] and Flock *et al.* [31], respectively. However, early measurements of the effective attenuation coefficient seem more reliable because they compare well with calculated values based on later measurements of μ_a and $\mu_s(1 - g)$.

Noticeable variations are present among the listed reduced scattering coefficients. The "added-absorber" technique produced $\mu_s(1 - g)$ values of 7.0 and 8.0 cm^{-1} for bovine and chicken muscles, respectively, at 633 nm. These are higher than those obtained using total diffuse and transmission measurements [42], [54] and from fluence measurements with isotropic detectors [58]. Ironically, the low anisotropy factor of 0.3 and scattering coefficient of 7.9 cm^{-1} for bovine muscle by Marijnissen is the reason that his value for $\mu_s(1 - g)$ was comparable with other values listed in Table III.

Diffusion theory [13], [62], [63] and the "added absorber" technique [14] were used to estimate the effective attenuation coefficient from interstitial light measurements in bovine muscles. They yielded values of 4.3–6.9 cm^{-1} which are higher than the 2.7 cm^{-1} obtained by Marijnissen and Star [37] using isotropic detectors. The 3.9 cm^{-1} reported by Kariagannes is within the range of the above two sets of results.

Doiron reports that rabbit muscle *in vivo* attenuates more 630 nm light than *in vitro* samples. Doiron measured values of 1.6–2.3 cm^{-1} *in vivo* but 1.1–1.5 cm^{-1} *in vitro* for the effective attenuation coefficient [12]. These differences might be due to perfusion of the *in vivo* samples. However, effective attenuation measurements of 2.6–4.8 cm^{-1} *in vivo* and 2.7–12.5 cm^{-1} *post mortem* by Wilson [35] did not exhibit any such difference in attenuation.

D. General Observations

This paper has emphasized the importance of matching experimental conditions with the theoretical model used to determine the optical properties. Reliability of optical properties depends on both theoretical *and* experimental techniques. For example, Kubelka–Munk measurements are questionable because the theoretical model is flawed and the experimental measurements are difficult to perform properly (infinite irradiation width, small diffuse reflection signal, and difficulty obtaining uniformly diffuse irradiances). Judgements of experimental accuracy are difficult, because many different tissue preparations and measurement parameters are involved. Preuss and Bolin [64] have reported a 39% and a 160% change in transmission from prefreezing at 488 and 515 nm, respectively. Such changes may translate into significant errors in the computed optical properties.

In this compilation, most measurements used a laser source. Little has been presented about optical properties measured as a function of wavelength using a spectrophotometer. There are optical property spectra for murine skin [15], cadaveric aorta [48], [65], murine liver [53], and human brain [66]. In the past, spectrophotometric data suffered from several errors. Typically, Beer's law was used to analyze transmission measurements, which is inapplicable if the samples scatter light or if the sample thickness is greater than the average scattering distance. When both spectrophotometric transmission and reflection data were available, Kubelka–Munk theory was used. Usually the data was not corrected for mismatched boundary conditions or pseudo-collimation of the irradiation source. Prahl [2] has described a procedure for matching spectrophotometer measurements to iterative computations of reflection and transmission to obtain μ_a and $\mu_s(1 - g)$. Undoubtedly careful calibration and use of the spectrophotometer with an integrating sphere can produce absorption and reduced scattering coefficients as a function of wavelength.

VI. Conclusion

Optical properties of biological tissues are vital to dosimetry studies. An up-to-date compilation of existing absorption, scattering, and anisotropy parameters accompanied by their associated theory and macroscopic measurements have been presented. Broad ranges in optical properties for any specific tissue are frequent, indicating the sensitivity and vulnerability of such measurements to variations in samples, detection apparatus, boundary conditions, and the governing light propagation model. The reliability of the reported values can be compromised by any of these factors.

Acknowledgment

The authors acknowledge all investigators whose work contributed to this review, and in particular thank W. Star for his "effective" remarks.

REFERENCES

[1] S. Chandrasekhar, *Radiative Transfer*. New York: Dover, 1960.

[2] S. A. Prahl, "Light transport in tissue," Ph.D. dissertation, Univ. Texas at Austin, 1988.

[3] H. C. van de Hulst, *Multiple Light Scattering, Volume 2*. New York: Academic, 1980.

[4] A. Ishimaru, *Wave Propagation and Scattering in Random Media, Volume 1*. New York: Academic, 1978.

[5] W. M. Star, "Comparing the P3-approximation with diffusion theory and with Monte Carlo calculations of light propagation in a slab geometry," *Proc. SPIE*, vol. IS5, Dosimetry of Laser Radiation in Medicine and Biology, G. J. Müller and D. H. Sliney, Eds., pp. 146–154, 1989.

[6] H. C. van de Hulst, *Multiple Light Scattering, Volume 1*. New York: Academic, 1980.

[7] E. P. Shettle and J. A. Weinman, "The transfer of solar irradiance through inhomogeneous turbid atmospheres evaluated by Eddington's approximation," *J. Atmos. Sci.*, vol. 27, pp. 1048–1055, 1970.

[8] J. H. Joseph, W. J. Wiscombe, and J. A. Weinman, "The delta-Eddington approximation for radiative flux transfer," *J. Atmos. Sci.*, vol. 33, pp. 2452–2459, 1976.

[9] G. Yoon, "Absorption and scattering of laser light in biological media—Mathematical modeling and methods for determining optical properties," Ph.D. dissertation, Univ. Texas at Austin, 1988.

[10] S. A. Prahl, J. W. Valvano, M. J. C. van Gemert, and A. J. Welch, "Boundary conditions and phase functions in the diffusion approximation of the radiative transport equation," *Appl. Opt.*, 1990 (submitted).

[11] L. O. Svaasand, D. R. Doiron, and A. E. Profio, "Light distribution in tissue during photoradiation therapy," USC Instit. Phys. Imaging Sci., USC-IPIS 900-02, 1981.

[12] D. R. Doiron, L. O. Svaasand, and A. E. Profio, "Light dosimetry in tissue applications to photoradiation therapy," in *Porphyrin Photosensitization*, D. Kessel and T. J. Dougherty, Eds. New York: Plenum, 1983, pp. 63–75.

[13] L. E. Preuss, F. P. Bolin, and B. W. Cain, "Tissue as a medium for laser light transport—Implications for photoradiation therapy," *Proc. SPIE*, vol. 357, Lasers in Surgery and Medicine, M. Berns, Ed., pp. 77–84, 1982.

[14] B. C. Wilson, M. S. Patterson, and D. M. Burns, "Effect of photosensitizer concentration in tissue on the penetration depth of photoactivating light," *Lasers Med. Sci.*, vol. 1, pp. 235–244, 1986.

[15] S. L. Jacques and S. A. Prahl, "Modeling optical and thermal distributions in tissue during laser irradiation," *Lasers Surg. Med.*, vol. 6, pp. 494–503, 1987.

[16] M. J. C. van Gemert, A. J. Welch, W. M. Star, M. Motamedi, and W. F. Cheong, "Tissue optics for a slab geometry in the diffusion approximation," *Lasers Med. Sci.*, vol. 2, pp. 295–302, 1987.

[17] G. Yoon, S. A. Prahl, and A. J. Welch, "Accuracies of the diffusion approximation and its similarity relations for laser irradiated biological media," *Appl. Opt.*, vol. 28, pp. 2250–2255, 1989.

[18] H. C. van de Hulst, *A New Look at Multiple Scattering*. New York: NASA Instit. Space Studies, 1962.

[19] G. N. Plass, G. W. Kattawar, and F. E. Catchings, "Matrix operator theory of radiative transfer. 1: Rayleigh scattering," *Appl. Opt.*, vol. 12, pp. 314–329, 1973.

[20] P. Kubelka, "New contributions to the optics of intensely light-scattering materials. Part I," *J. Opt. Soc. Amer.*, vol. 38, pp. 448–457, 1948.

[21] P. Kubelka, "New contributions to the optics of intensely light-scattering materials. Part II: Nonhomogeneous layers," *J. Opt. Soc. Amer.*, vol. 44, pp. 330–335, 1954.

[22] J. T. Atkins, "Optical properties of turbid materials," in *The Biologic Effects of Ultraviolet Radiation (with Emphasis on the Skin)*, F. Urbach, Ed. Oxford: Pergamon, 1969, pp. 141–150.

[23] F. Kottler, "Turbid media with plane-parallel surfaces," *J. Opt. Soc. Amer.*, vol. 50, pp. 483–490, 1960.

[24] P. S. Mudgett and L. W. Richards, "Multiple scattering calculations for technology," *Appl. Opt.*, vol. 10, pp. 1485–1502, 1971.

[25] W. E. Meador and W. R. Weaver, "Diffusion approximation for large absorption in radiative transfer," *Appl. Opt.*, vol. 18, pp. 1204–1208, 1979.

[26] K. Klier, "Absorption and scattering in plane parallel turbid media," *J. Opt. Soc. Amer.*, vol. 62, pp. 882–885, 1972.

[27] M. J. C. van Gemert and W. M. Star, "Relations between the Kubelka-Munk and the transport equation models for anisotropic scattering," *Lasers Life Sci.*, vol. 1, pp. 287–298, 1987.

[28] B. J. Brinkworth, "On the theory of reflection by scattering and absorbing media," *J. Phys. D: Appl. Phys.*, vol. 4, pp. 1105–1106, 1971.

[29] B. J. Brinkworth, "Interpretation of the Kubelka-Munk coefficients in reflection theory," *Appl. Opt.*, vol. 11, pp. 1434–1435, 1972.

[30] W. M. Star, J. P. A. Marijnissen, and M. J. C. van Gemert, "Light dosimetry in optical phantoms and in tissues: I. Multiple flux and transport theory," *Phys. Med. Biol.*, vol. 33, pp. 437–454, 1988.

[31] S. T. Flock, B. C. Wilson, and M. S. Patterson, "Total attenuation coefficients and scattering phase functions of tissues and phantom materials at 633 nm," *Med. Phys.*, vol. 14, pp. 835–841, 1987.

[32] B. C. Wilson, M. S. Patterson, and S. T. Flock, "Indirect versus direct techniques for the measurement of the optical properties of tissues," *Photochem. Photobiol.*, vol. 46, pp. 601–608, 1987.

[33] J. Eichler, J. Knof, and H. Lenz, "Measurements on the depth of penetration of light (0.35–1.0 μm) in tissue," *Rad. Environ. Biophys.*, vol. 14, pp. 239–242, 1977.

[34] B. C. Wilson and M. S. Patterson, "The physics of photodynamic therapy," *Phys. Med. Biol.*, vol. 31, pp. 327–360, Apr. 1986.

[35] B. C. Wilson, W. P. Jeeves, and D. M. Lowe, "*In vivo* and *post mortem* measurements of the attenuation spectra of light in mammalian tissues," *Photochem. Photobiol.*, vol. 42, pp. 153–162, 1985.

[36] I. Driver, J. W. Feather, P. R. King, and D. Gibson, "*In vivo* light dosimetry in interstitial photoradiation therapy (PRT)," *Proc. SPIE*, Int. Soc. of Opt. Eng. OE'Lase 88, M. Berns, Ed., pp. 98–102, 1988.

[37] J. P. A. Marijnissen and W. M. Star, "Phantom measurements for light dosimetry using isotropic and small aperture detectors," in *Porphyrin Localization and Treatment of Tumors*, D. R. Doiron and C. J. Gomer, Eds. New York: Alan R. Liss, pp. 133–148, 1984.

[38] J. P. A. Marijnissen and W. M. Star, "Quantitative light dosimetry *in vitro* and *in vivo*," *Lasers Med. Sci.*, vol. 2, pp. 235–242, 1987.

[39] A. L. McKenzie and P. O. Byrne, "Can photography be used to measure isodose distribution of space irradiance for laser photoradiation therapy?" *Phys. Med. Biol.*, vol. 33, pp. 113–131, 1988.

[40] G. H. M. Gjisbers, M.S. thesis, Eindhoven Univ., Eindhoven, The Netherlands, 1985.

[41] M. R. Arnfield, J. Tulip, and M. S. McPhee, "Optical propagation in tissue with anisotropic scattering," *IEEE Trans. Biomed. Eng.*, vol. 35, pp. 372–381, 1988.

[42] S. Andreola, A. Bertoni, R. Marchesini, and E. Melloni, "Evaluation of optical characteristics of different human tissues *in vitro*," *Lasers Surg. Med.*, vol. 8, p. 142 (abstract), 1988.

[43] R. Marchesini, A. Bertoni, S. Andreola, E. Melloni, and A. E. Sichirollo, "Extinction and absorption coefficients and scattering phase functions of human tissues *in vitro*," *Appl. Opt.*, vol. 28, pp. 2318–2324, 1989.

[44] F. H. Long, N. S. Nishioka, and T. F. Deustch, "Measurement of the optical and thermal properties of biliary calculi using pulsed photothermal radiometry," *Lasers Surg. Med.*, vol. 7, pp. 461–466, 1987.

[45] J. S. MacLeod, D. Blanc, and M. J. Colles, "Measurement of the optical absorption coefficients at 1.06 μm of various tissues using the photoacoustic effect," *Lasers Surg. Med.*, vol. 8, p. 143 (abstract), 1988.

[46] M. S. Patterson, B. Chance, and B. C. Wilson, "Time resolved reflectance and transmittance for the non-invasive measurement of tissue optical properties," *Appl. Opt.*, vol. 28, pp. 2331–2336, 1989.

[47] P. A. Wilksch, F. Jacka, and A. J. Blake, "Studies of light propagation in tissue," in *Porphyrin Localization and Treatment of Tumors*, D. R. Doiron and C. J. Gomer, Eds. New York: Alan R. Liss, 1984, pp. 149–161.

[48] M. Keijzer, R. R. Richards-Kortum, S. L. Jacques, and M. S. Feld, "Fluorescence spectroscopy of turbid media: autofluorescence of the human aorta," *Appl. Opt.*, vol. 28, pp. 4286–4292, 1989.

[49] M. J. C. van Gemert, R. Verdaasdonk, E. G. Stassen, G. A. C. M. Schets, G. H. M. Gijsbers, and J. J. Bonnier, "Optical properties of human blood vessel wall and plaque," *Lasers Surg. Med.*, vol. 5, pp. 235–237, 1985.

[50] A. A. Oraevsky, V. S. Letokhov, S. E. Ragimov, V. G. Omel'Yanenko, A. A. Belyaev, B. V. Shekhonin, and R. S. Akchurin, "Spectral properties of human atherosclerotic blood vessel walls," *Lasers Life Sci.*, vol. 2, pp. 275–288, 1988.

[51] G. D. Pedersen, N. J. McCormick, and L. O. Reynolds, "Transport calculations for light scattering in blood," *Biophys. J.*, vol. 16, pp. 199–207, 1976.

[52] L. O. Reynolds, C. C. Johnson, and A. Ishimaru, "Diffuse reflectance from a finite blood medium: Applications to the modeling of fiber optic catheters," *Appl. Opt.*, vol. 15, pp. 2059-2067, 1976.
[53] P. Parsa, S. L. Jacques, and N. S. Nishioka, "Optical properties of rat liver between 350 and 2200 nm," *Appl. Opt.*, vol. 28, pp. 2325-2330, 1989.
[54] J. L. Karagiannes, Z. Zhang, B. Grossweiner, and L. I. Grossweiner, "Applications of the 1-D diffusion approximation to the optics of tissues and tissue phantoms," *Appl. Opt.*, vol. 28, pp. 2311-2317, 1989.
[55] G. Mie, "Pioneering mathematical description of scattering by spheres," *Ann. Phys.*, vol. 25, p. 337, 1908.
[56] J. M. Steinke and A. P. Shepherd, "Diffusion model of the optical absorbance of whole blood," *J. Opt. Soc. Amer.*, vol. 5, pp. 813-822, 1988.
[57] L. O. Reynolds and N. J. McCormick, "Approximate two-parameter phase function for light scattering," *J. Opt. Soc. Amer.*, vol. 70, pp. 1206-1212, 1980.
[58] S. L. Jacques, C. A. Alter, and S. A. Prahl, "Angular dependence of HeNe laser light scattering by human dermis," *Lasers Life Sci.*, vol. 1, pp. 309-333, 1987.
[59] J. P. A. Marijnissen, W. M. Star, J. L. van Delft, and N. A. P. Franken, "Light intensity measurements in optical phantoms and *in vivo* during HpD photoradiation treatment using a miniature light detector with isotropic response," in *Photodynamic Therapy of Tumors and Other Diseases*, G. Jori and C. Perria, Eds. Padova, Italy: Libreria Progetto, 1985, pp. 387-390.
[60] W. F. Cheong, "Photo-thermal processes in tissue irradiated by Nd:YAG laser (1.06 μm, 1.32 μm)," Ph.D. dissertation, Univ. Texas at Austin, Dec. 1990.
[61] W. M. Star, J. P. A. Marijnissen, and M. J. C. van Gemert, "Light dosimetry: Status and prospects," *J. Photochem. Photobiol. B: Biology*, vol. 1, pp. 149-167, 1987.
[62] D. R. Doiron, L. O. Svaasand, and A. E. Profio, "Wavelength and dosimetry considerations in photoradiation therapy (PRT)," *Proc. SPIE*, vol. 357, Lasers in Surgery and Medicine, M. Berns, Ed., 1982.
[63] F. P. Bolin, L. E. Preuss, R. C. Taylor, and T. S. Sandu, "A study of the three-dimensional distribution of light (632.8 nm) in tissue," *IEEE J. Quantum. Electron.*, vol. QE-23, pp. 1734-1738, 1987.
[64] L. E. Preuss and F. P. Bolin, "Letter to the editor," *Lasers Life Sci.*, vol. 1, pp. 335-336, 1987.
[65] S. A. Prahl, A. J. Welch, M. P. Sartori, P. D. Henry, R. Roberts, G. L. Valderrama, K. Y. Jong, and M. J. Berry, "Optical properties of normal human aorta from 200 to 2200 nanometers," *Lasers Surg. Med.*, vol. 8, p. 142 (abstract), 1988.
[66] H. J. C. M. Sterenborg, M. J. C. van Gemert, W. Kamphorst, J. G. Wolbers, and W. Hogervorst, "The spectral dependence of the optical properties of the human brain," *Lasers Med. Sci.*, vol. 4, pp. 221-227, 1989.
[67] A. E. Profio and D. R. Doiron, "Transport of light in tissue in photodynamic therapy," *Photochem. Photobiol.*, vol. 46, pp. 591-599, 1987.
[68] G. I. Bell and S. Glasstone, *Nuclear Reactor Theory*. Malabar, FL: Robert E. Krieger, 1985.
[69] W. G. Houf and F. P. Incorpera, "An assessment of techniques for predicting radiation transfer in aqueous media," *J. Quantum Spec. Rad. Trans.*, vol. 23, pp. 101-115, 1980.
[70] B. C. Wilson and G. Adam, "A Monte Carlo model for the absorption and flux distributions of light in tissue," *Med. Phys.*, vol. 10, pp. 824-830, 1983.
[71] M. Keijzer, S. L. Jacques, S. A. Prahl, and A. J. Welch, "Light distributions in artery tissue: Monte Carlo simulations for finite-diameter laser beams," *Lasers Surg. Med.*, vol. 9, pp. 148-154, 1989.
[72] W. M. Star, J. P. A. Marijnissen, H. Jansen, M. Keijzer, and M. J. C. van Gemert, "Light dosimetry for photodynamic therapy by whole bladder wall irradiation," *Photochem. Photobiol.*, vol. 46, pp. 619-624, 1987.
[73] R. Splinter, W. F. Cheong, M. J. C. van Gemert, and A. J. Welch, "*In vitro* optical properties of human and canine brain and urinary bladder tissues at 633 nm," *Lasers Surg. Med.*, vol. 9, pp. 37-41, 1989.
[74] W. F. Cheong, M. Motamedi, and A. J. Welch, "Optical modeling of laser photocoagulation of bladder tissue," *Lasers Surg. Med.*, vol. 7, pp. 72 (abstract), 1987.
[75] L. O. Svaasand and R. Ellingsen, "Optical properties of human brain," *Photochem. Photobiol.*, vol. 38, pp. 293-299, 1983.
[76] L. O. Svaasand, C. J. Gomer, and A. E. Profio, "Laser-induced hyperthermia of ocular tumors," *Appl. Opt.*, vol. 28, pp. 2280-2287, 1989.
[77] L. O. Svaasand and R. Ellingsen, "Optical penetration in human intracranial tumors," *Photochem. Photobiol.*, vol. 41, pp. 73-76, 1985.
[78] H. Key, P. C. Jackson, and P. N. T. Wells, "Light scattering and propagation in tissue," *Poster Presentation, World Cong. Med. Phys., Bioeng.*, San Antonio, TX, Aug. 1988.
[79] S. Watanabe, T. J. Flotte, D. J. McAuliffe, and S. L. Jacques, "Putative photoacoustic damage in skin induced by pulsed ArF excimer laser," *J. Invest. Derm.*, vol. 90, pp. 761-766, 1988.
[80] R. Splinter, *Poster Presentation, Future Directions Lasers in Surg., Med., Eng. Foundat.* Florida, Feb. 1989.
[81] M. J. C. van Gemert, M. C. Berenbaum, and G. H. M. Gijsbers, "Wavelength and light-dose dependence in tumor phototherapy with hematoporphyrin-derivative," *Brit. J. Cancer*, vol. 52, pp. 43-49, 1985.
[82] B. C. Wilson, P. J. Muller, and J. C. Yanche, "Instrumentation and light dosimetry for intra-operative photodynamic therapy (PDT) of malignant brain tumors," *Phys. Med. Biol.*, vol. 31, pp. 125-133, 1986.
[83] P. J. Muller and B. C. Wilson, "An update on the penetration depth of 630 nm light in normal and malignant human brain tissue *in vivo*," *Phys. Med. Biol.*, vol. 31, pp. 1295-1297, 1986.
[84] R. R. Anderson and J. A. Parrish, "The optics of human skin," *J. Invest. Dermatol.*, vol. 77, pp. 13-19, 1981.
[85] M. J. C. van Gemert, A. J. Welch, and A. P. Amin, "Is there an optimal laser treatment for portwine stains?" *Lasers Surg. Med.*, vol. 6, pp. 76-83, 1986.
[86] S. Wan, R. R. Anderson, and J. A. Parrish, "Analytical modeling for the optical properties of the skin with *in vitro* and *in vivo* applications," *Photochem. Photobiol.*, vol. 34, pp. 493-499, 1981.

Wai-Fung Cheong was born in Malaysia. She received the B.Sc.(Hons.) degree in physics from the University of Malaya in June 1979 and the Diploma in education in December 1979. She was with Texas Tech University, Lubbock, as a Rotary Foundation Graduate Fellow, where she received the M.E. degree in clinical engineering in 1982.

In 1984 she began her doctoral studies at the University of Texas, Austin. She is currently a Research Assistant with special interests in the theoretical and empirical determination of laser-tissue interactive mechanisms, applied specifically to photocoagulation in urological oncology and laser angioplasty.

Scott A. Prahl, for a biography, see this issue, p. 2304.

Ashley J. Welch (M'66-SM'79), for a biography and photograph, see this issue, p. 2239.